Molecular Second-Order Optical Nonlinearities of Metallocenes

Joseph C. Calabrese,[†] Lap-Tak Cheng,*[,†] Jennifer C. Green,[‡] Seth R. Marder,*[,§,∥] and Wilson Tam[†]

Contribution from the Central Research and Development Department, E. I. du Pont de Nemours & Company, Inc., Experimental Station, P.O. Box 80356, Wilmington, Delaware 19880-0356, Inorganic Chemistry Laboratory, Oxford University, South Parks Road, Oxford OX1 3QR, England, Jet Propulsion Laboratory, California Institute of Technology, 4800 Oak Grove Drive, Pasadena, California 91109, and Molecular Materials Resource Center, The Beckman Institute, California Institute of Technology, Pasadena, California 91125. *Received February 4, 1991. Revised Manuscript Received May 16, 1991*

Abstract: The nonresonant quadratic molecular hyperpolarizabilities of several ferrocene and ruthenocene derivatives were studied by dc electric-field-induced second-harmonic generation (EFISH) experiments using fundamental radiation at 1.91 μm. Hyperpolarizabilities approaching that of 4-(dimethylamino)-4′-nitrostilbene (DANS) were observed, indicating that the ferrocene moiety can act as an effective donor. It was found that the dipole projections of the β tensors of ferrocene complexes are comparable to those of methoxyphenyl systems with similar acceptors. Thus, (*E*)-ferrocenyl-4-(4-nitrophenyl)ethylene (**5**) has a β value of 31×10^{-30} esu whereas 4-methoxy-4′-nitrostilbene has a value for β of 29×10^{-30} esu. Replacement of the iron atom with ruthenium, which has a higher ionization potential, leads to a reduction in β relative to **5**. Replacement of a cyclopentadienyl ring with a pentamethylcyclopentadienyl ring leads to increased nonlinearity.

Introduction

There is considerable interest in the synthesis of new materials with large second-order optical nonlinearities because of their potential use in device applications related to telecommunications, optical computing, optical storage, and optical information processing.[1-3] Materials with large second-order hyperpolarizabilities (β) are needed in order to realize many of these applications. Large second-order hyperpolarizabilities are associated with structures that have large differences between ground-state and excited-state dipole moments.[4] Furthermore, β is largest when the transition dipole moments between these states are large and the energy gap between them is small.[4-6] Molecules with π-donor–π-acceptor interactions are promising candidates to fulfill the above requirements. For organic compounds, structure–property trends concerning donor–acceptor strengths and the effectiveness of different conjugated backbones have been topics of many studies.[7] Our recent efforts have provided an extensive set of internally consistent results on many of the important molecular classes.[8] Organometallic and coordination compounds allow us to explore new variables for the engineering of nonlinear optical (NLO) hyperpolarizabilities. We can change the transition-metal element, is oxidation state, and the number of d electrons to examine the differences between diamagnetic and paramagnetic complexes and the effect of new bonding geometries and coordination patterns. There are several reasons to speculate that organometallic and coordination compounds may give rise to new and enhanced optical nonlinearities:

(1) These compounds can have metal to ligand or ligand to metal charge-transfer bands in the UV–visible region of the spectrum. These optical absorption bands are often associated with large second-order optical nonlinearities.

(2) Chromophores containing metals, such as phthalocyanines, are among the most *intensely* colored materials known. The *strength* of the optical absorption band (that is related to its transition dipole moment) is also associated with large optical nonlinearities.

(3) Organometallic and coordination compounds are often strong oxidizing or reducing agents, since metal centers may be electron rich or poor depending on their oxidation state and ligand environment. Thus, the metal center may be an extremely strong donor or acceptor.

(4) Metals can be used to fine-tune the electronic properties of organic fragments.

In contrast to the wealth of information available regarding the NLO properties of organic molecules, there are few data on organometallic compounds. Initial efforts[9-15] to evaluate the potential of organometallic compounds for quadratic nonlinear optics have been restricted to the Kurtz second-harmonic-gen-

[†] E. I. du Pont de Nemours & Co., Inc.
[‡] Oxford University.
[§] Jet Propulsion Laboratory, California Institute of Technology.
[∥] The Beckman Institute, California Institute of Technology.

(1) Williams, D. J. *Angew. Chem., Int. Ed. Engl.* **1984**, *23*, 690.
(2) *Nonlinear Optical Properties of Organic and Polymeric Materials*; Williams, D. J., Ed.; ACS Symposium Series 233; American Chemical Society: Washington, DC, 1983.
(3) *Nonlinear Optical Properties of Organic Molecules and Crystals*: Chemla, D. S., Zyss, J., Eds.; Academic: Orlando, FL, 1987; Vols. 1 and 2.
(4) Oudar, J. L.; Chemla, D. S. *J. Chem. Phys.* **1977**, *66*, 2664.
(5) Levine, B. F.; Bethea, C. G. *J. Chem. Phys.* **1977**, *66*, 1070.
(6) Lalama, S. J.; Garito, A. F. *Phys. Rev. A* **1979**, *20*, 1179.
(7) For example: (a) Nicoud, J. F.; Twieg, R. J. In ref 3, p 255 and references therein. (b) Huijts, R. A.; Hesselink, G. L. J. *Chem. Phys. Lett.* **1989**, *156*, 209. (c) Barzoukas, M.; Blanchard-Desce, M.; Josse, D.; Lehn, J.-M.; Zyss, J. *Chem. Phys.* **1989**, *133*, 323.
(8) (a) Cheng, L. T.; Tam, W.; Meredith, G. R.; Rikken, G.; Meijer, E. W. *Proc. SPIE-Int. Soc. Opt. Eng.* **1989**, *1147*, 61. (b) Cheng, L. T.; Tam, W.; Feiring, A.; Rikken, G. L. J. A. *Proc. SPIE-Int. Soc. Opt. Eng.* **1990**, 1337. (c) Cheng, L. T.; Tam, W.; Stevenson, S. H.; Meredith, G. R.; Rikken, G. L. J. K.; Marder, S. R. *J. Phys. Chem.*, submitted for publication. (d) Cheng, L. T.; Tam, W.; Marder, S. R.; Stiegman, A. E.; Rikken, G. L. J. K.; Spangler, C. W. *J. Phys. Chem.*, submitted for publication. (e) Tiemann, B. G.; Marder, S. R.; Perry, J. W.; Cheng, L. T. *Chem. Mater.* **1990**, *2*, 690. (f) Marder, S. R.; Beratan, D. N.; Cheng, L.-T. *Science* **1991**, *252*, 103.
(9) Frazier, C. C.; Harvey, M. A.; Cockerham, M. P.; Hand, H. M.; Chauchard, E. A.; Lee, C. H. *J. Phys. Chem.* **1986**, *90*, 5703.
(10) Eaton, D. F.; Anderson, A. G.; Tam, W.; Wang, Y. *J. Am. Chem. Soc.* **1987**, *109*, 1886.
(11) (a) Green, M. L. H.; Marder, S. R.; Thompson, M. E.; Bandy, J. A.; Bloor, D.; Kolinsky, P. V.; Jones, R. J. *Nature* **1987**, *330*, 360. (b) Bandy, J. A.; Bunting, H. E.; Green, M. L. H.; Marder, S. R.; Thompson, M. E.; Bloor, D.; Kolinsky, P. V.; Jones, R. J. In *Organic Materials for Non-linear Optics*; Hann, R. A., Bloor, D., Eds.; Royal Society of Chemistry Special Publication No. 69; Royal Society of Chemistry: London, 1989; pp 219–224.
(12) (a) Calabrese, J. C.; Tam, W. *Chem. Phys. Lett.* **1987**, *133*, 244. (b) Anderson, A. G.; Calabrese, J. C.; Tam, W.; Williams, I. D. *Chem. Phys. Lett.* **1987**, *134*, 392. (c) Tam, W.; Calabrese, J. C. *Chem. Phys. Lett.* **1988**, *144*, 79. (d) Tam, W.; Wang, Y.; Calabrese, J. C.; Clement, R. A. *SPIE Proc.-Int. Soc. Opt. Eng.* **1988**, *971*, 107.
(13) Bandy, J. A.; Bunting, H. E.; Garcia, M. H.; Green, M. L. H.; Marder, S. R.; Thompson, M. E.; Bloor, D.; Kolinsky, P. V.; Jones, R. J. In *Organic Materials for Non-linear Optics*; Hann, R. A., Bloor, D., Eds.; Royal Society of Chemistry Special Publication No. 69; Royal Society of Chemistry: London, 1989; pp 225–231.
(14) Coe, B. J.; Jones, C. J.; McCleverty, J. A.; Bloor, D.; Kolinsky, R. J. *J. Chem. Soc., Chem. Commun.* **1989**, 1485.
(15) Marder, S. R.; Perry, J. W.; Schaefer, W. P.; Tiemann, B. G.; Groves, P. C.; Perry, K. J. *SPIE Proc.-Int. Soc. Opt. Eng.* **1989**, *1147*, 108.

0002-7863/91/1513-7227$02.50/0

eration (SHG) powder test.[16] We found that (Z)-1-ferrocenyl-2-(4-nitrophenyl)ethylene (1) has an SHG efficiency 62 times that of urea[11a] and the related salt (E)-1-ferrocenyl-2-(N-methylpyridinium-4-yl)ethylene iodide (2) has an SHG efficiency roughly 220 times that of urea, the largest efficiency known for an organometallic compound.[15] These results demonstrate that organometallic compounds can exhibit large $\chi^{(2)}$.

The magnitude of the SHG signals obtained from the Kurtz powder test is largely determined by crystallographic, linear optical (i.e. birefringence), and dispersive factors; therefore, little insight into molecular structure–property relationships can be inferred.[1] Solution-phase dc electric-field-induced second-harmonic generation.[17] (EFISH) is a more appropriate method for hyperpolarizability studies. EFISH provides direct information on vectorial projection (β) of the hyperpolarizability tensor along the molecular dipole (μ) direction. When the dominant charge-transfer (CT) axis and the dipolar axis are roughly collinear, the β determined by EFISH is a measure of the intrinsic nonlinearity of a molecule, assuming experiments are carried out with radiation of sufficiently long wavelength, such that dispersive contributions to the observed SHG signal are negligible. However, there remain important limitations that should be mentioned. First, the rich coordination patterns and ligand structures of organometallic compounds may make interpretation of EFISH results impossible if the molecule lacks a clear CT axis. However, tensorial components only partially active in EFISH may be important in determining bulk properties for such compounds. Second, the EFISH response comprises two parts:

$$\gamma_i^{\mathrm{EFISH}} = \gamma_i^{e} + \gamma_i^{\nu} + \frac{\mu\beta}{5kT} \qquad (1)$$

where i = 1 and 2, denoting the solvent and solute contributions. There is a rotational dipolar part, which is due to the $\mu\beta$ product; however, there is a second part, $\gamma^e + \gamma^\nu$, which is the deformational term summing electronic and hyper-Raman contributions to the EFISH signal. This second term may be significant as a result of the large polarizability of metal-containing compounds. Correction for this electronic contribution can be made by using data obtained from third-harmonic generation experiments, when material absorption permits.[8]

We are developing a detailed understanding of structural factors that govern intrinsic molecular hyperpolarizabilities of organic and organometallic compounds using EFISH and third-harmonic-generation (THG) measurements.[8,18] The low oxidation potential generally observed for ferrocene complexes and the stability of α-ferrocenyl-substituted carbocations lead us to speculate that ferrocene would be an effective charge-transfer (CT) donor for NLO systems.[19,20] These factors and the large observed powder efficiencies of several ferrocene complexes[11,14,15] motivated us to characterize β for a series of metallocene complexes. A preliminary communication has been published.[21] In this full paper, we report the details of our EFISH measurements, syntheses, and molecular orbital calculations of ferrocene and ruthenocene derivatives. We emphasize that our goal was to probe the effect of systematic structural variations on β, *not to find optimized high-β molecules.*

Results and Discussion

The donor strength of the metallocene naturally will be dependent on the oxidation potential of the metal center and additional substituents on both five-membered rings. We therefore have studied structural variations including different metal centers, Z and E isomers, symmetric electron-donating substituents in the form of pentamethylcyclopentadienyl rings (Cp*) as well as extension of conjugation, and variation of the acceptor group; the formulations of the compounds studied and β values are summarized in Tables I and II. Compounds 3 and 4 (Table I) represent the cyclopentadienyl analogues of acceptor-substituted benzenes. Compounds 1 and 5–10 (Table II) have structural resemblance to some previously studied acceptor-substituted stilbenes.[8a]

Table I. Summary of Linear and Nonlinear Optical Data for Metallocenes of the Form $(C_5X_5)M(C_5H_4Y)$[a]

compd	M	X	Y	μ, 10^{-18} esu	α, 10^{-23} esu	β, 10^{-30} esu	γ, 10^{-36} esu
3	Fe	H	$COCH_3$	3.0	2.6	0.3 ± 0.2	27
4	Ru	Me	NO_2	5.5	3.9	0.6 ± 0.2	

[a] All values of μ are ±0.3 × 10^{-18} esu. The uncertainties in the values of α, β, and γ are ±10% of the reported values.

Scheme I

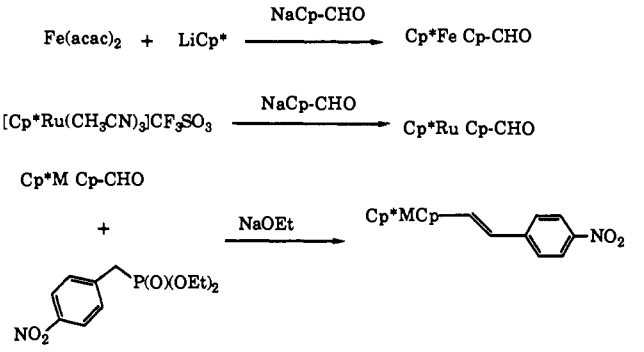

Preparation of Metallocenes. New metallocenes prepared for this study are compounds 4, 6, 10, and 11 (see Tables I and II). The reaction of diethyl (p-nitrobenzyl)phosphonate with (Cp–CHO)M (Cp = cyclopentadienyl) yielded for Cp* (6), Ru (10), and Cp*Ru (11) analogues of 5. The syntheses are summarized in Scheme I. Cp*FeCp–CHO was generated in situ from the reaction of $Fe(acac)_3$ (acac = acetylacetonate) with LiCp* and NaCp–CHO.[22] Reaction of Cp*FeCp–CHO with diethyl (p-nitrobenzyl)phosphonate yielded compound 6. Compound 11 was similarly prepared from the reaction of the diethyl (p-nitrobenzyl)phosphonate with the analogous Ru compound. The mixed metallocenes, Cp*RuCp–CHO and Cp*RuCp–NO_2, were prepared by treating $[Cp^*Ru(CH_3CN)]CF_3SO_3$[23] with NaCp–CHO[22] and LiCp–NO_2,[24] respectively. Compound 4 can also be prepared from the reaction of LiCp–NO_2 with $[Cp^*RuCl]_4$.[23] Preparation of mixed metallocenes from $[Cp^*Ru(CH_3CN)_3]$-CF_3SO_3 has been reported.[25] Compound 10 was prepared from the reaction of CpRuCp–CHO with diethyl (p-nitrobenzyl)-phosphonate.

Due to the paucity of structural information on nitrocyclopentadienyl–metal complexes, the X-ray structure of 4 was determined. The Cp–NO_2 group is not perfectly planar; the torsion angle between the plane formed by the Cp ring and the nitro group is 2.3°. Additional information on the structure of 4 is available in the supplementary material.

Nonlinear Optical Studies. The low-energy spectra of simple metallocenes are dominated by two weak bands at 325 and 440 nm (the 440-nm band is actually two unresolved bands) for ferrocene and 277 and 321 nm for ruthenocene.[26,27] The spectrum changes dramatically upon substitution of the Cp ring with conjugated and/or acceptor groups. For example, in the spectrum

(16) Kurtz, S. K.; Perry, T. T. *J. Appl. Phys.* **1968**, *39*, 3798.
(17) Levine, B. F.; Bethea, C. G. *Appl. Phys. Lett.* **1974**, *24*, 445.
(18) Cheng, L.-T.; Tam, W.; Eaton, D. F. *Organometallics* **1990**, *9*, 2857.
(19) Kuwana, T.; Bublitz, D. E.; Hoh, G. L. K. *J. Am. Chem. Soc.* **1960**, *82*, 5811.
(20) Turbitt, T. D.; Watts, W. E. *J. Chem. Soc. B* **1971**, 177.
(21) Cheng, L.-T.; Tam, W.; Meredith, G. R.; Marder, S. R. *Mol. Cryst. Liq. Cryst.* **1990**, *189*, 137.
(22) Hart, W. P.; Macomber, D. W.; Rausch, M. D. *J. Am. Chem. Soc.* **1980**, *102*, 1196.
(23) (a) Fagan, P. J.; Ward, M. D.; Calabrese, J. C. *J. Am. Chem. Soc.* **1989**, *111*, 1698. (b) Fagan, P. J.; Ward, M. D.; Casper, J. V.; Calabrese, J. C.; Krusic, P. J. *J. Am. Chem. Soc.* **1988**, *110*, 2981.
(24) Rausch, M. D.; Hart, W. P. *J. Organomet. Chem.* **1980**, *197*, 225.
(25) Burk, M. J.; Arduengo, A. J., III; Calabrese, J. C.; Harlow, R. L. *J. Am. Chem. Soc.* **1989**, *111*, 8938.
(26) For example: Rosenblum, M. *Chemistry of the Iron Group Metallocenes*: Wiley Interscience: New York, 1965; Chapter 2.
(27) Sohn, Y. S.; Hendrickson, D. N.; Gray, H. B. *J. Am. Chem. Soc.* **1971**, *93*, 3603.

Table II. *Summary of Linear and Nonlinear Optical Data for Metallocenes of the Form* $(C_5X_5)M(C_5H_4)-(CH{=}CH)_n-p-C_6H_4Y$[a]

compd	M	X	*n*	isomer	Y	λ_{CT}, nm	μ, 10^{-18} esu	α, 10^{-23} esu	β, 10^{-30} esu[a]	γ, 10^{-36} esu
5	Fe	H	1	*E*	NO_2	356/496	4.5	3.9	31	
1	Fe	H	1	*Z*	NO_2	325/480	4.0	3.8	13	
6	Fe	Me	1	*E*	NO_2	366/533	4.4	5.3	40	
7	Fe	H	1	*E*	CN	324/466	4.6	3.8	10	
8	Fe	H	1	*Z*	CN	308/460	3.9	3.8	4.0	
9	Fe	H	1	*E*	CHO	338/474	3.9	3.8	12	
10	Ru	H	1	*E*	NO_2	350/390	5.3	4.2	12	114
11	Ru	Me	1	*E*	NO_2	370/424	5.1	5.0	24	140
12	Fe	H	2	*E,E*	NO_2	382/500	4.5	4.6	66	

[a] All values of μ are $\pm 0.3 \times 10^{-18}$ esu. The uncertainties in the values of α, β, and γ are $\pm 10\%$ of the reported values.

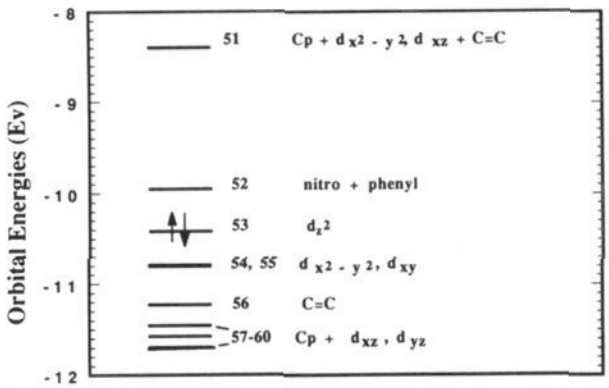

Figure 1. Energy level diagram for the frontier molecular orbitals of **5** from extended Hückel molecular orbital calculations.

of **2** in acetonitrile, there are two bands in the visible region: one at λ_{max} = 380 nm (ϵ = 29 000 M^{-1} cm^{-1}); the second at λ_{max} = 550 nm (ϵ = 8000 M^{-1} cm^{-1}).[28] Similar bathochromic shifts are observed for the ruthenocene derivatives, but they are, in general, less pronounced. These changes are best understood in terms of the changes of the molecular orbital picture upon substitution of the Cp with conjugated acceptors. The bonding in ferrocene is well understood.[26,27] Eight electrons reside in four strongly bonding orbitals that are largely π ring-orbital in character. Four electrons occupy two bonding orbitals, which provide the key d–π interactions between the ring e_{1g} and the metal d_{xz} and d_{yz} orbitals. The remaining six electrons fill the largely nonbonding MOs, which are essentially the d_{z^2} (a_{1g}), and the d_{xy} and $d_{x^2-y^2}$ (e_{2g}) orbitals of the metal center. Although there remains disagreement on their relative order, d_{z^2} is generally accepted as the HOMO of ferrocene. The LUMO is a combination of the metal d_{xz} and d_{yz} (e_{1g}) orbitals, and above this lie metal Cp antibonding orbitals derived from Cp π^* orbitals. The low-energy bands in the electronic spectrum of ferrocene are assigned to a $^1A_{1g}$–$^1E_{2g}$ and two $^1A_{1g}$–$^1E_{1g}$ ligand field transitions.[26,27] Upon substitution of the Cp with conjugated acceptors, qualitatively one would expect the low-lying π^* ligand orbitals to shift to lower energy and there would be increased mixing of the ligand orbitals with the metal d orbitals. Extended Hückel molecular orbital calculations on **5** provide insight into the nature of these optical bands and the chemical bonding in substituted metallocenes. Figure 1 shows an energy level scheme for the frontier orbitals, and Figure 2 shows selected orbitals of **5**. The HOMO (orbital 53) is almost completely d_{z^2} in nature, with the next lower energy occupied orbitals (54 and 55) being $d_{x^2-y^2}$ and d_{xy}. These orbitals are essentially nonbonding. Immediately below the d orbitals lie several orbitals (56–60) that are closely spaced in energy and have substantial π-ligand character, with some metal character. Though the extended Hückel calculation is expected to provide a good model for the general localization of orbitals, the calculated orbital energies are very sensitive to the parametrization and are not expected to be more than a very approximate guide to the energies of transitions. The spacing of the occupied orbitals corresponds

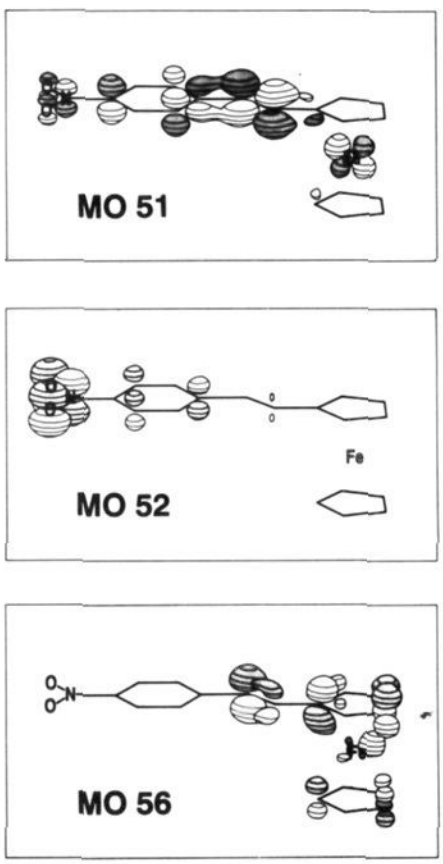

Figure 2. Orbital diagrams showing (top) orbital 56, (middle) orbital 52, and (bottom) orbital 51, from extended Hückel molecular orbital calculations on **5**.

well with ionization energy data on these materials,[29] so we are reasonably confident of the presence of two significant low-lying occupied molecular orbitals with the localizations shown for orbitals 51 and 52 (Figure 2). The LUMO (orbital 52) is largely localized on the nitro group, and the next highest unfilled orbital (51) has coefficients distributed throughout the π ligand with some metal character. We therefore tentatively assign the lowest energy transition in these systems as a metal (53–55) to ligand (51) CT band and the higher energy transition as being effectively a ligand π (56–60) to π^* (52) transition, *with some metal character.* Although it is possible that the lowest energy transition may be from orbitals 53–55 to orbital 52, we believe that this is rather unlikely since the overlap between these orbitals is rather small. Electron density is substantially redistributed in both transitions, and therefore *both* transitions are likely to contribute to β. Solvatochromic behavior has been observed for compounds **5** and **6**. The lower lying bands are bathochromically shifted about 8–10 nm, and the higher lying bands are shifted somewhat less between *p*-dioxane and acetonitrile solutions, indicative of increased polarity

(28) Marder, S. R.; Perry, J. W.; Schaefer, W. P.; Tiemann, B. G. *Organometallics* **1991**, *10*, 1896.

(29) Bunting, H. E. D. Phil. Thesis, Oxford University, 1989.

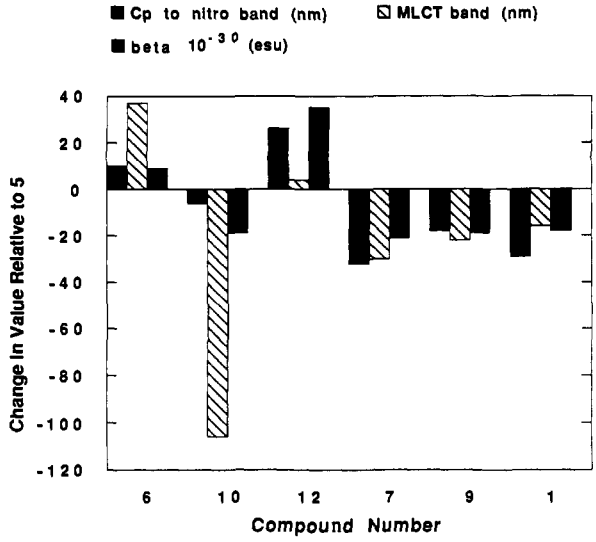

Figure 3. Bar graph representation of the changes in the absorbance maxima and β values for selected metallocenes, relative to compound **5**.

in the Franck–Condon excited state. The π–π^* CT transition is analogous to the CT transition in donor/acceptor-substituted benzenes where electron densities move from a filled, bonding π orbital of benzene perturbed by the donor (here the iron atom) to an empty low-lying orbital of the substituent. The lowest energy MLCT transition is fundamentally different because an electron almost completely localized in one orbital is transferred upon excitation. The donated electron density involved in both charge-transfer (CT) bands depends strongly on the metal center, and it is not valid to consider the metal center as a counterion merely providing a full electron to form a five-member aromatic Cp anion. We expect the higher energy band to be more sensitive to variations in the extended π system and the lower energy band to be more sensitive to changes at the metal center. With compound **5** as a reference, pentamethyl substitution of one ring leads to 36- and 10-nm bathochromic shifts of the lower and higher energy bands, respectively (Figure 3). Replacement of iron by ruthenium lowers the energy of the nonbonding d orbitals, thus increasing the metal's oxidation potential and lowering its donating strength. As expected, the lower energy band is hypsochromically shifted by 106 nm but the higher energy band is only shifted by 6 nm. In contrast, the higher energy band of (*E*,*E*)-1-ferrocenyl-4-(4-nitrophenyl)butadiene (**12**) is shifted bathochromically (26 nm) relative to **5** and the lower energy band shifts slightly (4 nm) (Figure 3). Variation of the acceptor strength affects both the π–π^* CT and the MLCT transition, as expected (see compounds **7** and **9** in Figure 3).

Compounds **3** and **4** show somewhat larger dipole moments but substantially lower β values compared to their benzene analogues. The dipole moment of the ruthenium compound **4** is particularly high, given a value of only 4.0 D for nitrobenzene. Two independent factors could contribute to the large dipole moment of this compound. First, the electron-releasing Cp* enhances the donor strength of the metal center and therefore to the acceptor-substituted Cp as well.[30] The importance of this effect is not clear for compounds **5** vs **6** and **10** vs **11**, as they have the same dipole moments within experimental error. The second factor is the greater orbital extent of ruthenium 4d vs iron 3d orbitals, which could perhaps stabilize more charge transfer in the ground state (**10** vs **5** and **11** vs **6**). This latter rationale has been used to explain the increased stability of α-ruthenocenyl cations relative to α-ferrocenyl cations.[20]

The low β values for compounds **3** and **4** may be due to the poorly defined CT axes since the metal–ring bond is perpendicular to the ring–substituent bond. Other derivatives (Table II) that have well-defined charge-transfer axes along the (4-nitrophenyl)vinyl group show respectable nonlinearities, in comparison to roughly analogous organic compounds, e.g. nitrostilbene (β = 9.1 × 10^{-30} esu), 4-methoxy-4′-nitrostilbene (β = 2.9 × 10^{-30} esu), and 4-(dimethylamino)-4′-nitrostilbene (β = 75 × 10^{-30} esu).[8a] Since these compounds have long-wavelength absorption bands, the measured nonlinearity has a small dispersive enhancement. Compound **1** (*Z* isomer) is found to be less nonlinear than compound **5** (*E* isomer); likewise, **8** has a smaller β than **7**. It is expected that the *Z* isomer would exhibit lower β for two reasons: (1) the steric interactions between the Cpα and benzene ortho hydrogens preclude the two rings being coplanar (this was seen in the crystal structure of **1**[11a]), resulting in a diminution of coupling between the donor and the acceptor; (2) the through-space distance between the donor and the acceptor is less in the *Z* isomer than in the *E* isomer; therefore, the change in dipole moment per unit charge separation will be less. Compound **1** crystallizes in space group *F*2*dd*; in this space group, phase-matched SHG will be optimized when the angle between the largest tensor component of β and the polar crystallographic axis is 54.74°.[31] The modest value of β for **1** (β = 13 × 10^{-30} esu) suggests that the herringbone pattern formed by the crystallographically related Fe to nitro vectors in the solid state is largely responsible for the relatively large observed powder SHG value.[11a]

Recently, Zerner intermediate neglect of differential overlap (ZINDO) calculations were performed on several of the compounds in this study and the calculated values of β were in excellent agreement with those EFISH-determined values. Interestingly, the authors suggest that only the π–π^* CT transition contributes to the observed nonlinearity.[32] If this is the case, one might not expect structural changes that only affect the characteristics of the lower energy MLCT band to have a substantial effect on the magnitude of the observed nonlinearity. Yet the permethylated compounds **6** (Figure 3) and **11** exhibit a significant increase in nonlinearity as compared to their Cp analogues, **5** and **10**. These trends may result from the destabilization of the high-lying occupied orbitals as evidenced by the large spectral red shift of the MLCT transition and lowered oxidation potentials.[26] Furthermore, despite the fact that the π–π^* CT bands of the ruthenium compounds **10** (Figure 3) and **11** shift 6 nm or less relative to those of their iron analogues, **5** and **6**, the former compounds are less nonlinear than their iron counterparts. These observations are consistent with the higher energy MLCT transitions and oxidation potential[26] of ruthenocene compounds (vs ferrocene compounds). Thus, these structural modifications, which have a large effect on the MLCT transition and a much smaller effect on the higher energy π–π^* CT transition, appear to influence the magnitude of the observed nonlinearity. In agreement with structural trends observed in stilbene derivatives, the effect of increased conjugation length is dramatic, with compound **12** exhibiting significantly higher β than **5** (Figure 3). The changes in β as a function of acceptor strength parallel those observed for donor/acceptor-substituted stilbenes, with stronger acceptors leading to higher β. For a given metallocene fragment, β appears to correlate with the oxidation potential of the complex.[33] This is reasonable, since increasing the strength of the acceptor is expected to both increase the nonlinearity of the complex and decrease the electron density of the metal center in the the ground state. However when the acceptor (*p*-nitrophenyl) is kept constant and the metallocene fragment is varied, β scales inversely with the redox potential of the complex. This suggests that the energy of the filled metal orbitals correlates with β.

Our conclusions may be summarized as follows: (1) Structural variations that affect the π–π^* CT *and* the MLCT transitions lead to changes in β. Since both transitions appear to make substantial contributions to the observed nonlinearity, it is not appropriate to use the two-state model, when considering metallocenes, such as those discussed here. The energy and extinction

(30) Richmond, H. H.; Freiser, H. *J. Am. Chem. Soc.* **1955**, *77*, 2022.

(31) Zyss, J.; Oudar, J. L. *Phys. Rev. A* **1982**, *26*, 2028.

(32) Kanis, D. R.; Ratner, M. A.; Marks, T. J. *J. Am. Chem. Soc.* **1990**, *112*, 8203.

(33) Toma, S.; Gaplovsky, A.; Elecko, P. *Chem. Pap.* **1985**, *39*, 115.

coefficients of both bands are sensitive to changes about the metal center (the MLCT band being more sensitive). The results therefore demonstrate that the *metal center plays an important role in determining the nonlinear polarizabilities* of these molecules. (2) The dipole projections of the β tensors of ferrocene and ruthenocene complexes are compared to those of methoxyphenyl systems with like acceptors. (3) On the basis of binding energies and redox potentials alone, the molecular hyperpolarizabilities might be expected to be larger than the observed values. *We believe that poor coupling between the metal center and the substituent because of the π geometry most likely lowers the effectiveness of the metal center as a donor.* We therefore suggest that future studies of organometallic systems for both second- and third-order hyperpolarizabilities should focus on improving the coupling between the metal center and the organic fragment by incorporating the metal in the same plane as the π system and perhaps introducing some metal to carbon multiple-bond character.

Experimental Section

Syntheses. The compounds **1**,[11a] **5**,[11b,32] **7**,[11b,33] **8**,[11b] **9**,[11b,23] **12**,[11b] $Fe(acac)_2$,[34] $(C_5H_5)Ru(C_5H_4CHO)$,[35] $[(C_5(CH_3)_5)Ru(CH_3CN)_3]CF_3SO_3$,[23] NaC_5H_4CHO,[22] and $LiC_5H_4NO_2$[24] were prepared according to literature procedures. Compound **3** was obtained from Aldrich Chemical Co. and was used without further purification.

Preparation of 6. To 1.29 g of $Fe(acac)_2$ (5.08 mmol) in 30 mL of tetrahydrofuran (THF) was added a slurry of 0.672 g (4.74 mmol) of LiCp* in 30 mL of THF. The mixture was stirred for 15 min, and 0.550 g (4.74 mmol0 of NaCp–CHO in 20 mL of THF was added. The mixture was stirred overnight and then filtered. After the solid was washed with ether, the solvent was removed. The residue was extracted with CH_2Cl_2 and the mixture filtered. The solvent was removed, and 15 mL of ethanol was added. To this mixture was added 1.29 g (4.73 mmol) of $(O)P(OC_2H_5)_2CH_2$-*p*-$C_6H_4NO_2$ in 10 mL of ethanol. The resulting mixture was cooled in an ice bath, and freshly prepared $NaOC_2H_5$ (from 0.110 g of Na in 10 mL of ethanol) was added. The mixture was then warmed to room temperature and stirred for 2 days. The solvent was removed and the residue chromatographed on silica gel eluted with 50% $CHCl_3$/hexane. A yellow band was collected, followed by a purple band. The purple band yielded 0.905 g (2.2 mmol, 47%) of the product as a blue-black solid. Anal. Calcd for $C_{23}H_{25}NO_2Fe$: C, 68.50; H, 6.25. Found: C, 68.07, 67.82; H, 6.30, 6.28. ^1H NMR (CD_2Cl_2): δ 8.16 (d, J = 8.8 Hz, 2 H), 7.55 (d, J = 8.8 Hz, 2 H), 6.96 (d, J = 16.0 Hz, 1 H), 6.63 (d, J = 16.0 Hz, 1 H), 4.00 (m, 4 H), 1.83 (s, 15 H). SHG was inactive at 1.9 μm.

In a separate experiment, treatment of $Fe(acac)_2$ with LiCp* and NaCp–CHO gave a 2:1 mixture of Cp*FeCp–CHO and $(Cp^*)_2Fe$. To 0.600 g (2.36 mmol) of $Fe(acac)_2$ in 20 mL of THF was added 0.336 g (2.36 mmol) of LiCp* in 10 mL of THF. After the mixture was stirred for 0.5 h, 0.275 g (2.36 mmol) of NaCp–CHO in 10 mL of THF was added. The resulting mixture was stirred overnight and then filtered, after which the solvent was removed. The residue was extracted with CH_2Cl_2, the mixture filtered, and the solvent removed. For the mixture of Cp*FeCp* and Cp*FeCp–CHO, the ^1H NMR spectrum in CD_2Cl_2 indicates about a 2.1:1 mixture. ^1H NMR of Cp*FeCp–CHO: δ 9.66 (s), 4.15 (m), 4.21 (m), 1.8 (s).

Preparation of 10. To 0.500 g (1.93 mmol) of CpRuCp–CHO and 0.527 g (1.93 mmol) of $(O)P(OC_2H_5)_2CH_2$-*p*-$C_6H_4NO_2$ in 10 mL of ethanol, cooled in an ice bath, was added freshly prepared $NaOC_2H_5$ (from 45 mg of Na in 2 mL of ethanol). After the mixture was stirred overnight, the product was filtered off and washed with ethanol. A yield of 0.63 g was obtained (1.66 mmol, 86%). Anal. Calcd for $C_{18}H_{15}NO_2Ru$: C, 57.14; H, 4.00. Found: C, 56.91; H, 4.22. ^1H NMR (CD_2Cl_2): δ 8.15 (m, 2 H), 7.5 (m, 2 H), 7.0 (d, J = 16.1 Hz, 1 H), 6.7 (d, J = 16.1 Hz, 1 H), 4.86 and 4.63 (A_2B_2 t, 2 H and 2 H), 4.5 (s, 15 H). SHG was inactive at 1.06 μm.

Preparation of Cp*Ru–CpCHO. To 0.614 g (1.21 mmol) of $[Cp^*Ru(CH_3CN)_3]CF_3SO_3$ in 15 mL of THF was added 0.154 g (1.33 mmol) of NaCp–CHO in 10 mL of THF. The mixture was stirred overnight. The solvent was then removed and the residue chromatographed on silica gel eluted with $CHCl_3$. A yellow band was collected to give 0.374 g (1.13 mmol, 93.8%) of the product. ^1H NMR (CD_2Cl_2): δ 9.38 (s, 1 H), 4.52 (m, 2 H), 4.63 (m, 2 H), 1.86 (s, 15 H). Anal. Calcd for $C_{16}H_{20}ORu$: C, 58.34; H, 6.12. Found: C, 58.08; H, 6.01. IR (KBr): 1677 cm^{-1}.

Preparation of 11. To 0.316 g (0.96 mmol) of Cp*RuCp–CHO in 10 mL of ethanol was added 0.260 g (0.95 mmol) of $(O)P(OC_2H_5)_2CH_2$-*p*-$C_6H_4NO_2$. The mixture was cooled in an ice bath, and freshly prepared $NaOC_2H_5$ (from 21 mg of Na in 5 mL of ethanol) was added. The resulting mixture was stirred overnight and the solvent removed. The residue was chromatographed on silica gel eluted with $CHCl_3$ to give 0.245 g of the product as an orange-yellow solid. Anal. Calcd for $C_{23}H_{25}RuNO_2$: C, 61.59; H, 5.62. Found: C, 61.70; H, 5.70. ^1H NMR (CD_2Cl_2): δ 8.14 (m, 2 H), 7.5 (m, 2 H), 6.8 (d, J = 16 Hz, 1 H), 6.5 (d, J = 16 Hz, 1 H), 4.5 (t, J = 1.7 Hz, 2 H), 4.36 (t, J = 1.7 Hz, 2 H), 1.8 (s, 15 H). SHG was inactive at 1.06 μm.

Preparation of 4. To 0.300 g (0.2767 mmol) of $[Cp^*RuCl]_4$ in 15 mL of THF at −78 °C was added 0.150 g (1.28 mmol) of LiCp–NO_2. The mixture was warmed to room temperature and stirred overnight under nitrogen. The solvent was removed, and the residue was chromatographed on silica gel eluted with 50% $CHCl_3$/hexane to give 0.133 g of the product. Anal. Calcd for $C_{15}H_{19}NO_2Ru$: C, 52.01; H, 5.53. Found: C, 52.22; H, 5.68. ^1H NMR (CD_2Cl_2): δ 5.15 (m, 2 H), 4.5 (m, 2 H), 1.8 (s, 15 H). The x-ray structure was determined from crystals grown from hexane.

Alternative Preparation of 4. To 500 mg (0.98 mmol) of $[Cp^*Ru(CH_3CN)_3]CF_3SO_3$ in 15 mL of THF at −78 °C was added 0.150 g (1.3 mmol) of LiCp–NO_2 in 10 mL of THF. The mixture was warmed to room temperature and stirred overnight. The solvent was then removed, and the residue was chromatographed on silica gel eluted with 50% $CHCl_3$/hexane to give 0.198 g (0.57 mmol, 58%) of the desired product.

EFISH Measurements. To extract the molecular hyperpolarizability, β, a lengthy set of physical and optical measurements needed to be carried out. These included measurements of density, refractive index at several wavelengths, solution capacitance, and THG and EFISH amplitudes and coherence lengths (for both SHG and THG) for a series of solutions with graded concentrations. These measurements respectively determined the specific volume of a solute molecule in solution, solution dispersion, solution dielectric properties, and the THG and EFISH nonlinear susceptibilities for each solution. The details of our experimental methodology and data analysis have been given elsewhere.[8a,36] We briefly describe a few key features of our experiments in this section.

The experimental setup consists of a 20-Hz Nd:YAG laser with 10-ns pulses of 0.4 J in energy. The 1.06-μm output pumps a hydrogen Raman shifter, providing up to 120 mW of Stokes-shifted radiation at 1.91 μm. This radiation serves as the fundamental frequency for both the EFISH and THG experiments, with the harmonic wavelengths at 954 and 636 nm, respectively. For most lightly colored compounds with absorption edges at wavelengths below 500 nm, the measurement can be considered as nondispersively enhanced. THG and EFISH experiments were carried out with an unconventional technique in which the harmonic amplitudes and coherence lengths were measured separately. The laser beam was divided three ways: an intensity normalization reference branch, a coherence length measurement branch, and a harmonic amplitude measurement branch. The second and third harmonic signals from all three branches were separated with dichroic mirrors, detected with photomultiplier tubes, and collected through gated integrators.

For the determination of harmonic amplitudes, we adopted a tight focusing geometry to place the focal region of the laser beam at the window–liquid interface of a "single-interface" sample cell. The sample cell was equipped with a thick (2 cm) front optical window and two adjacent liquid chambers (3-cm path length) holding a reference liquid and a sample solution for comparative measurement. Electrodes were fabricated at the front window–liquid interface so that both THG and EFISH measurements could be carried out concurrently. The coherence lengths for the harmonic generations were determined with a wedged liquid cell consisting of two crystalline quartz windows, which generated sufficient second- and third-harmonic radiations for easy measurement. Our goal was to eliminate possible environmental contributions, which were known to be important in THG and, to a lesser extent, in EFISH measurements[37] and to increase the measurement precision by eliminating the necessity of simultaneously extracting several parameters from data fitting as is the case for the conventional Maker's fringe or wedge techniques. All experimental procedures and data acquisition scheme is were optimized to allow efficient and accurate measurements.

Figure 4 shows typical EFISH/THG amplitude (top) and dispersion (bottom) data. The amplitude data show the EFISH (○) and THG (◇)

(34) (a) Paciello, R. A.; Manriquez, J. M.; Bercaw, J. E. *Organometallics* **1990**, *9*, 260. (b) Bunnel, E. E.; Valle, L.; Manriquez, J. M. *Organometallics* **1985**, *4*, 1680.

(35) Bublitz, D. E.; McEwen, W. E.; Kleinberg, J. *J. Am. Chem. Soc.* **1962**, *84*, 1845.

(36) Meredith, G. R.; Cheng, L. T.; Hsiung, H.; Vanherzeele, H. A.; Zumsteg, F. C. *Materials for Nonlinear and Electro-optics*; Lyons, M. H., Ed.; The Institute of Physics (IOP Publishing): New York, 1989; p 139.

(37) (a) Meredith, G. R.; Buchalter, B.; Hanzlik, C. *J. Chem. Phys.* **1983**, *78*, 1533. (b) Meredith, G. R. *Opt. Commun.* **1981**, *39*, 89.

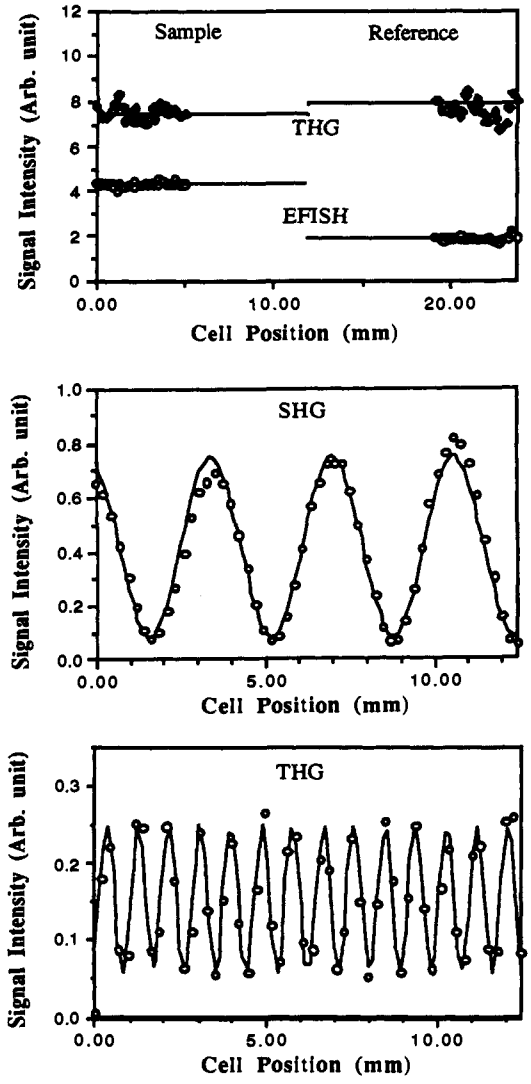

Figure 4. EFISH/THG amplitude (top), SHG dispersion (middle), and THG dispersion (bottom) data.

signals for an organic solution in the left chamber and for toluene in the right chamber. Clearly, the signal level (abscissa) is independent of the cell position (coordinate) within each chamber, demonstrating the lack of interference arising from harmonic generations at other interfaces. The solid lines represent calculated signal averages. The ratio of the harmonic intensities generated in the two chambers can be precisely determined. The dispersion data show the oscillatory periods from which coherence lengths can be extracted by knowing the wedge angle of the liquid cell. The SHG coherence length is much longer than that of THG, as expected. The nonzero background is a result of the focusing and finite spot size of the laser beam. The gradual rise in signal is a result of a slight wedge on one of the quartz windows. Solid lines are least-squares fits to determine the periods. With the known THG and EFISH nonlinearities and coherence lengths of the window material and the reference liquid (for BK7-grade A glass, $\chi^{(3)}_{THG} = 4.7 \times 10^{-14}$ esu, $l_{THG} = 16.7$ μm, $\chi^{(3)}_{EFISH} = 3.5 \times 10^{-14}$ esu, and $l_{EFISH} = 38.8$ μm; for toluene, $\chi^{(3)}_{THG} = 9.9 \times 10^{-14}$ esu, $l_{THG} = 18.3$ μm, $\chi^{(3)}_{EFISH} = 9.1 \times 10^{-14}$ esu, and $l_{EFISH} = 73.5$ μm),[38] as well as the coherence lengths of the sample solution, the solution nonlinear susceptibilities can be computed.

With the measured solution properties, following the full Onsager local field model[39] for both static and optical fields and taking the infinite-dilution limit[40] for all concentration-dependent quantities, we can calculate the relevant molecular properties including the dipole moment, μ, the low-frequency linear polarizability, α, the hyperpolarizability, β, and the second hyperpolarizability, γ. The effective refractive indices for the solute molecule in solution, as required by the Onsager model, are deduced from the solute-specific volumes and high-frequency polarizabilities. The vectorial component, β, of the molecular hyperpolarizability tensor along the dipole moment is calculated according to $\gamma^{EFISH} = \gamma^{e} + \gamma^{v} + \mu\beta/5kT$ where $\gamma^{e} + \gamma^{v}$, denoting a purely electronic and a hybrid vibrational contribution, is scaled with γ^{THG}. Where optical absorptions do not permit THG measurements, the electronic and vibrational contribution is taken to be 10%, which is a typical value found for the more quadratically nonlinear molecules.

Extended Hückel Calculations. Extended Hückel molecular orbital calculations[41] with charge iteration were carried out for **5**. The conjugated ligand was assumed to be planar with distances and bond angles taken from the crystal structure determination of **1**.[11a] Parameters used for the orbitals are given in Table III.

Table III. Parameters Used in the Extended Hückel Calculations

atom	orbital	exponents (ζ)[a]	energy,[b] eV
H	1s	1.300	−13.6 (−13.22 to −13.70)
C	2s	1.625	−21.40 (−20.29 to −21.72)
	2p	1.625	−11.40 (−10.49 to −11.07)
N	2s	1.950	−26.00 (−28.91)
	2p	1.950	−13.40 (−12.12)
O	2s	2.275	−32.30 (−28.71)
	2p	2.275	−14.80 (−12.12)
Fe	3d	5.35 (0.5505)	−12.6 (−10.73)
		2.00 (0.6260)	
	4s	1.9	−9.1 (−8.93)
	4p	1.9	−5.32 (−4.84)

[a] Double-ζ values were used for d orbitals. Coefficients are given in parentheses. [b] Values for the energies after charge interation are given in parentheses. For C and H the range of energies is given.

Acknowledgment. We thank H. Jones (du Pont), T. Hunt (du Pont), and B. G. Tiemann (JPL) for expert technical assistance. We also thank Dr. Joseph Perry and Bruce Tiemann (JPL) and Gerald R. Meredith (du Pont) for helpful discussions throughout the preparation of this paper. We also thank Dr. Paul Fagan (du Pont) for samples of $[(C_5(CH_3)_5)Ru(CH_3CN)_3]CF_3SO_3$ and Dr. Juan Manriquez (du Pont) for samples of $Fe(acac)_2$. The helpful comments of the reviewers are also gratefully acknowledged. The research described in this paper was performed, in part, by the Jet Propulsion Laboratory, California Institute of Technology, at its Center for Space Microelectronics Technology, which is supported by the Strategic Defense Initiative Organization, Innovative Science, and Technology Office through an agreement with the National Aeronautics and Space Administration.

Supplementary Material Available: For compound **4**, a textural presentation of the crystal data, data collection and treatment, and structure solution and refinement, Figures 1 and 2, showing an ORTEP drawing and a packing diagram with atom numbering, and tables of fractional coordinates, anisotropic thermal parameters, and complete distances and angles (5 pages). Ordering information is given on any current masthead page.

(38) (a) Buchalter, B.; Meredith, G. R. *Appl. Opt.* **1982**, *21*, 3221. (b) Stevenson, S. H. Unpublished results, 1988.

(39) For example: Bottcher, C. J. F. *Theory of Electric Polarization*, 2nd ed.; Elsevier: New York, 1973.

(40) Singer, K. D.; Garito, A. F. *J. Chem. Phys.* **1981**, *75*, 3572.

(41) Hoffmann, R.; Lipscomb, W. N. *J. Chem. Phys.* **1962**, *36*, 2179.